


# Influence of source parameters on the growth of metal nanoparticles by sputter-gas-aggregation

Malak Khojasteh<sup>1,2</sup> · Vitaly V. Kresin<sup>1</sup> 

Received: 24 July 2017 / Accepted: 1 November 2017 / Published online: 7 November 2017  
© The Author(s) 2017. This article is an open access publication

**Abstract** We describe the production of size-selected manganese nanoclusters using a magnetron sputtering/aggregation source. Since nanoparticle production is sensitive to a range of overlapping operating parameters (in particular, the sputtering discharge power, the inert gas flow rates, and the aggregation length), we focus on a detailed map of the influence of each parameter on the average nanocluster size. In this way, it is possible to identify the main contribution of each parameter to the physical processes taking place within the source. The discharge power and argon flow supply the metal vapor, and argon also plays a crucial role in the formation of condensation nuclei via three-body collisions. However, the argon flow and the discharge power have a relatively weak effect on the average nanocluster size in the exiting beam. Here the defining role is played by the source residence time, governed by the helium supply (which raises the pressure and density of the gas column inside the source, resulting in more efficient transport of nanoparticles to the exit) and by the aggregation path length.

**Keywords** Nanoparticles · Nanoclusters · Vapor aggregation · Mass spectrometry

## Introduction

To explore precisely how the properties and functionality of nanoscale particles depend on the number of constituent atoms, it is important to have tools which enable full control of particle size, purity, and shape. Consequently, surface deposition of size-selected metal nanoclusters has gained popularity for its ability to tune the particle size and composition over a wide range (Milani and Iannotta 1999; Meiwes-Broer 2000; Binns 2001; Wegner et al. 2006; Vajda and White 2015).

A powerful tool for generating beams of neutral and charged nanoclusters covering a range of sizes and materials is the sputtering/aggregation source, also sometimes referred to as the “terminated gas condensation” source (Haberland et al. 1992, 1994; Hutte 2017). It is based on the quenching of atomic vapor produced by magnetron sputtering of the material of interest. The vapor becomes supersaturated due to collisions with the surrounding inert gas atoms which are cooled by the cold walls of the aggregation zone, condenses into nanoclusters, and is carried out of the condensation chamber by a continuous flow of gas. This device has been adopted by many research groups and has evolved from a purely home-built instrument to a commercial thin-film deposition product.

Understanding the efficiency of cluster formation in a source of this type is obviously a nontrivial problem, because it involves the interplay between multiple processes, including (1) sputtering of atoms and ions, (2) emergence of condensation nuclei, (3) supersaturation and particle growth, (4) transport to the exit aperture and diffusion to the aggregation chamber walls, (5) expansion through the aperture into the process vacuum chamber, accompanied by the formation of the nanoparticle beam and termination of growth. Importantly, as nanoparticles

✉ Vitaly V. Kresin  
kresin@usc.edu

<sup>1</sup> Department of Physics and Astronomy, University of Southern California, Los Angeles, CA 90089-0484, USA

<sup>2</sup> Mork Family Department of Chemical Engineering and Materials Science, University of Southern California, Los Angeles, CA 90089-1211, USA

move with the gas through the source towards the exit aperture, their local environment continuously changes, adding a degree of non-equilibrium dynamics to the growth process.

Not surprisingly, therefore, the yield and size distribution of the resulting nanoparticle beam are functions of multiple interrelated operational parameters: source geometry, gas flow rates, discharge power and configuration, aggregation residence time, etc. Thus, to enhance particle production and to steer its size distribution toward the desired range, it is valuable to have both empirical and conceptual insights into the effect of these parameters on the cluster formation process. Many papers have examined the effect of operating conditions on the size, morphology, and kinetic energy of nanoclusters (examples include Hihara and Sumiyama 1998; Morel et al. 2003; Pratontep et al. 2005; Das et al. 2009; Quesnel et al. 2010; Ayesh et al. 2010; Gracia-Pinilla et al. 2010; Nielsen et al. 2010; Ganeva et al. 2012; Luo et al. 2012; Ayesh et al. 2013; Bray et al. 2014; Dutka et al. 2015; Fischer et al. 2015; Kusior et al. 2016; Zhao et al. 2016; Rudd et al. 2017), but each typically looked only at a subset of source parameters. Consequently, a comprehensive multidimensional characterization has not yet been presented.

In this paper, we describe a systematic study of the influence of the parameters of our source on the production of metal nanoclusters, using manganese as an example. Four independently controlled variables (argon and helium flow rates, discharge power, and aggregation length) were varied over a set of discrete levels (corresponding to a total of 720 four-dimensional grid points), and the effect of each combination on the cluster size distribution can be traced

and visualized with the help of contour plots. Such a map over the permutations and interplay of independent factors is sometimes referred to as a “factorial design” experiment. It allows us to consider and assign the key roles played by the individual parameters listed above, for example the distinct contributions of argon and helium gases to the processes of nanocluster formation and transport within the source. These assignments are supplemented by nanocluster beam velocity measurements.

## Experiment

Figure 1 shows the scheme of our experimental setup for the production of size-selected nanoclusters. The source is Nanogen-50 from Mantis Deposition Ltd. As mentioned above, nanoparticles are produced by magnetron (dc) sputtering followed by condensation within the environment of a cold inert gas. The magnetron block is equipped with “magnet set A” whose most useful feature, per company specifications, is that it produces almost exclusively ionized clusters (Mantis Deposition 2017), making it possible to filter and manipulate the entire beam by electric fields.

Clusters are generated from 99.95% Mn targets (ACI Alloys) of 2-in. diameter and 0.125-in. thickness, bonded onto a copper backing plate. The magnetron head is mounted on a linear translator, enabling the aggregation length (the distance between the target and the exit aperture) to be varied over a range of 10 cm. Argon and helium gases (both 99.999% purity) are introduced into the source region behind the magnetron head, with flow rates

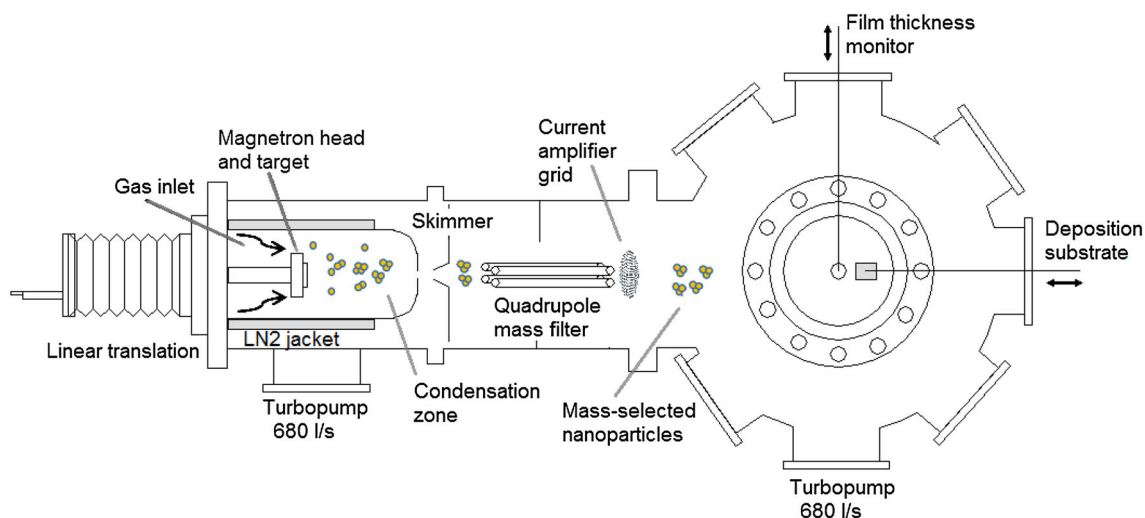


**Fig. 1** Apparatus schematic. In the magnetron/vapor condensation source, sputtered metal atoms enter the aggregation zone where they undergo collisions with the inert gas and quickly thermalize. Nanocluster ions form and grow, as the mixture moves through the

source toward the exit aperture. The ions are filtered by a quadrupole mass analyzer equipped with an ion flux measurement grid and enter the deposition chamber

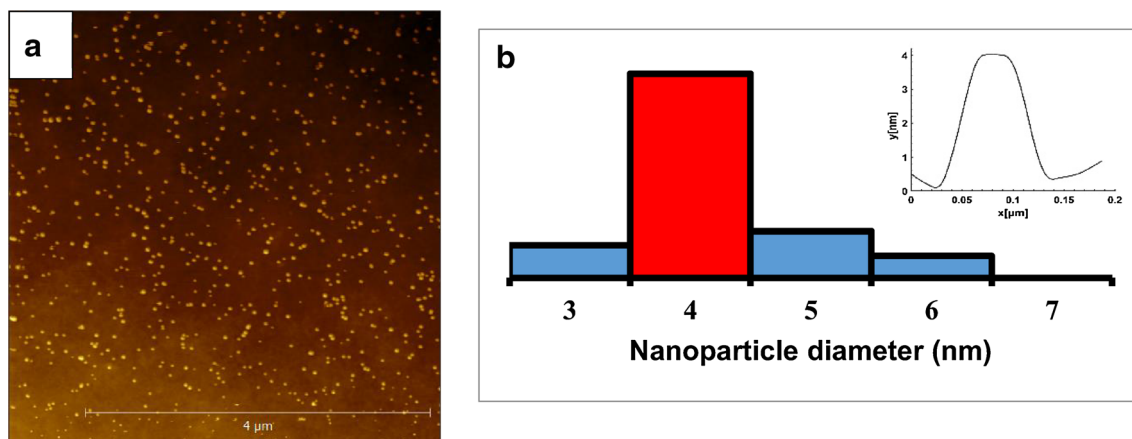


**Fig. 2** **a** Tapping mode AFM image of size-selected 4 nm diameter Mn nanoclusters deposited on a Si/SiO<sub>2</sub> substrate. **b** AFM profile of one individual nanoparticle from **a**, as well as a histogram of the

deposited particles' heights. Note that the transverse dimension appears artificially broadened due to tip size convolution

regulated by Alicat MC series mass flow controllers. The flow rate dependence of cluster production will be described below. Argon is used as the plasma discharge medium, and the roles of argon and helium in the nucleation and clustering process are further discussed below. The outer jacket of the source chamber is maintained full of liquid nitrogen with the help of a funnel filling system and a liquid level controller.

The gas carries the nanoclusters out of a 5-mm aperture at the source exit, where particle growth is terminated. The resulting directed beam passes through a 6-mm skimmer followed by a high-range/high throughput quadrupole mass filter (Mantis MesoQ, see also (Baker et al. 1997)) with a manufacturer stated size resolution of  $\sim 2\%$ . The standard mass range of the filter is from 350 amu to  $\sim 10^6$  amu, but its performance can be extended somewhat to either side of the standard range. A grid mounted at the quadrupole exit samples the ion flux and an electrometer, included in the mass spectrometer instrumentation package, measures the current corresponding to the selected cluster size. The resolution of the mass filter is selected by setting the  $U/V$  ratio (i.e., the ratio of the dc and ac amplitudes of the quadrupole's rod voltages) between 0.001 and 0.168; the  $rf$  frequency is then adjusted automatically by the MesoQ power supply and its control software. For the data reported below, the  $U/V$  ratio was kept at 0.02.

Upon passing through the quadrupole, the size-selected nanoclusters find themselves in the main deposition chamber (base pressure  $\sim 10^{-6}$  Pa). Here their mass deposition rate, as a function of size, can be measured using a quartz crystal film thickness oscillator (McVac Manufacturing) and monitor (Inficon XTC). In addition to the arrangement described in a preliminary report (Khojasteh and Kresin 2016), in this work the ion current impinging on the deposition surface can also be measured

by means of a picoammeter (Keithley 6487). A Faraday cup arrangement (see Appendix) can be positioned downstream from the quadrupole exit to measure the cluster ions' kinetic energies. Figure 2 shows, as an example, an atomic-force microscope (AFM) image and profile, and a height histogram, of nanoparticles soft-landed in the deposition chamber when the quadrupole mass spectrometer was set to a diameter of 4 nm. The close correspondence between the selected and imaged nanoparticle sizes confirms the accuracy of the mass filter.

## Results and discussion

As described above, the magnetron sputtering and cluster formation processes involve the interplay of many source parameters. In our work, the four main factors are the magnetron discharge power  $P$ , the aggregation length  $L$ , and the Ar and He gas flow rates  $Q_{\text{Ar}}$  and  $Q_{\text{He}}$ . The cluster beam distribution was traced over  $5 \times 3 \times 4 \times 12$  set levels of these variables, respectively, for a total of 720 outcome data points. Such a map enables us to examine both individual effects of the source parameters on the cluster beam distribution as well as, importantly, possible correlations which cannot be detected from separate one-way analyses.

### Argon and helium supply

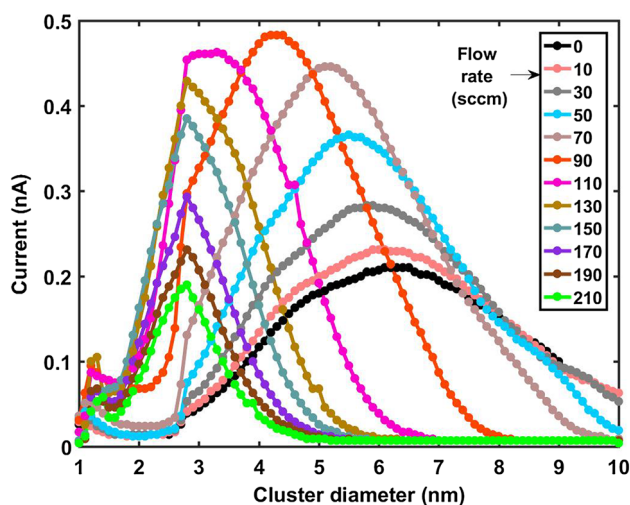
In dc magnetron sputtering, a high negative voltage is applied to the target, accelerating  $\text{Ar}^+$  ions to sputter material off the target (in our case, Mn) surface. Strong magnets positioned behind the target create a specially shaped magnetic field designed to lengthen electron paths in front of the target and intensify the plasma. In our

exploration of the parameter space, we first let in only argon gas to determine the dc power needed to produce a stable flux of Mn nanoclusters as detected by the quadrupole mass filter. This process was performed gradually to prevent target thermal shock possibly resulting in cracking or debonding from the backing plate. Once the discharge is established, the Ar flow rate can be increased further, and then He admixed gradually. In this way, the variation of cluster sizes as a function of both gas flow rates can be mapped out for a given discharge power and condensation length. We found that the size distribution is quite reproducible for each set of operating parameters.

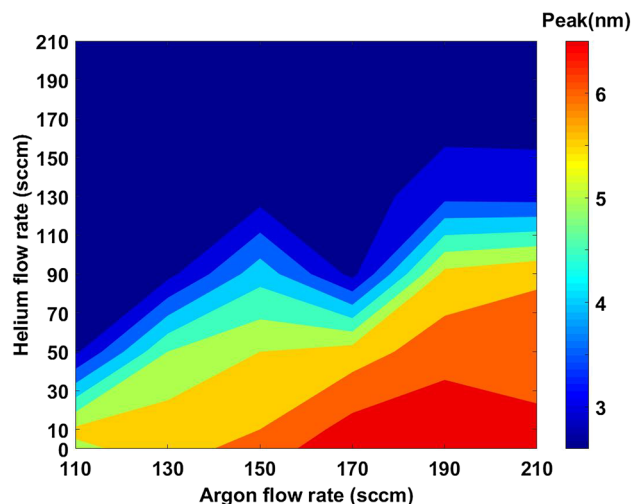
Initially, as the supply of pure argon is increased both the flux and the average size of the cluster ions grow, until finally a stable log-normal-type shape of the distribution becomes established. At this point, the helium supply is turned on, and the response of the nanoparticle beam to increasing helium flow is illustrated in Fig. 3: the overall intensity rises, reaches a maximum, and then starts to decrease, while the average particle size shifts to smaller sizes. At the same time, the width of the beam distribution becomes narrower.

Figure 4 puts the influence of both gases into perspective by simultaneously plotting the effect of Ar and He flows on the peak of the cluster beam distribution. With the helium supply fixed, increasing the argon flow has only a moderate influence on the average particle size. However (as already illustrated in Fig. 3), an increase in the helium flow shifts the beam distribution toward lower sizes very significantly.

How can one interpret these different (indeed, opposite) trends? It is evident that helium and argon perform distinct



**Fig. 3** Effect of He flow rate on the size distribution of Mn nanoclusters. All other source parameters are kept constant: aggregation length 9 cm, discharge power 21.8 W, Ar flow rate 150 sccm



**Fig. 4** Position of the peak of the Mn nanoparticle size distribution vs. Ar and He flow rates. The flow rates were measured at intervals of 20 sccm, and the values in-between interpolated. The discharge power was 22 W and the aggregation length was 9 cm

functions within the cluster source. Their roles and influences can be rationalized as follows:

As extensively described in the literature, the formation of nanoclusters  $M_n$  out of atomic vapor is initiated by nucleation and sustained by supersaturation and growth (see, e.g., Kappes and Leutwyler 1988; Haberland 1994; Pauly 2000; Smirnov 2000; Hutte 2017). The initial step is the formation of a bound dimer  $M_2$  which requires a three-body collision for stabilization:  $M + M + Ar \rightarrow M_2 + Ar$ . It is well-known that the heavier noble gas atoms are efficient at removing the dimer's binding energy, and helium is not nearly as effective at enabling nucleation. This is also why heavier carrier gases are better at promoting clustering in supersonic expansion sources (Kappes and Leutwyler 1988). The dimers then serve as condensation nuclei for further growth, if the vapor is maintained in a state of supersaturation. In this process, clusters grow by sequential condensation as additional atoms arrive at their surface one by one (with further collisions with noble gas atoms helpful in cooling the cluster seeds by removing the additional condensation energy). At higher nucleation densities, cluster–cluster collisions also can result in the appearance of larger particles. Particles which reach the so-called “critical size” will continue coagulating towards the condensed phase; therefore, if a population of finite-sized clusters is desired, then the condensation process must be interrupted. In the present source, this comes about as the gas flow carries the atomic vapor through the aperture and out of the condensation zone.

Now we can formulate the separate roles of the two noble gases supplied to the source. While the distinction obviously is not sharp, it enables useful qualitative interpretation and guidance.

As just stated, the size of nanoclusters in the beam is to a large degree controlled not by a hypothetical equilibrium distribution, but by the fact that the growth process is interrupted by the transit of the clusters out of the source (hence the aforementioned label “terminated gas condensation source”). The stage at which particle condensation is interrupted, and therefore the maximum size that is able to be attained, is defined by the residence time in the growth region, i.e., by the speed at which the metal vapor/inert gas mixture is swept from the sputtering area to the source exit aperture. It is this transport which appears to be mostly affected by the amount of helium flow into the source, in such a way that the average cluster size goes down as the helium supply increases.

In what way can the rate of helium gas supply influence the time a nanoparticle spends inside the source? It might be supposed that a higher mass flow,  $Q$ , translates into a greater speed of the gas column inside the source,  $v_{\text{gas}}$ , pulling the particles along and reducing their residence/growth time. However, this is mainly not the case. Indeed, in equilibrium, the gas mass flow through the source is  $Q = \rho_{\text{gas}} v_{\text{gas}} A$ , where  $\rho_{\text{gas}}$  is the gas mass density in the column and  $A$  is its effective cross section. At the same time,  $Q$  must equal the mass flow through the nozzle aperture into the vacuum chamber, which is proportional to the stagnation pressure in the plane of the nozzle (Miller 1988; Pauly 2000), and thereby to  $\rho_{\text{gas}}$ :  $Q \propto P_{\text{gas}} \propto \rho_{\text{gas}}$ . Comparing these two expressions, both of which involve  $\rho_{\text{gas}}$  but only one involves  $v_{\text{gas}}$ , we conclude that raising the inlet gas flow rate should mainly affect the pressure and density of the gas column inside the source but not its velocity.

Therefore, the likely reason for the reduction in average cluster size with greater He density inside the source is that the clusters become more effectively entrapped in the gas streamlines. This derives both (1) from the higher number of cluster collisions with the gas atoms in the column drifting to the exit aperture, and (2) from the fact that the rate of cluster diffusion toward the surrounding walls decreases inversely with the diffusion coefficient and therefore inversely with the gas density (Smirnov 2000; Shyjumon et al. 2006). As a result, the growing particles have a greater tendency to persist on their direct trajectories, their residence time decreases, and the growth is terminated sooner.

The fact that smaller cluster sizes are congruent with entrapment in the gas is also supported by velocity measurements on particles emerging from the source aperture, as described in the Appendix.

An increased supply of Ar contributes to cluster transport as well; however, it also performs the essential functions of (1) enabling the sputtering process, thereby feeding atoms and atomic ions into the vapor, and (2) facilitating

the appearance of condensation nuclei. Hence the argon density strongly affects the overall intensity of the nanoparticle beam, but its roles in supplying metal vapor for coagulation and in promoting cluster drift toward the source exit appear to balance each other out. As a result, the Ar flow rate does not have a sharp influence on the size distribution of the formed particles.

An alternative interpretation of the principal role of helium in a magnetron source was put forward by Prantep et al. (2005). They suggested that the helium gas is itself involved in cluster formation in such a way that, with increased He flow there is a rise in the nucleation of small seeds which results in more but smaller clusters. However, since argon is even more efficient in enabling the formation of small nuclei, under this scenario one might expect a stronger shift towards small sizes not just with He, but also with increasing Ar flow, which is not observed.

### Magnetron power and aggregation length

The dc sputtering discharge power strongly affects nanocluster production. In principle, the stronger the discharge the greater the supply of raw cluster material into the vapor; however, one also has to be cognizant of heat load limitations on the target as well as of discharge stability and plasma charging dynamics. In Fig. 5a, we examine the influence of power and helium flow rate on the peak of the beam size distribution. We see that in this representation, the helium supply again plays the most influential role.

Figure 5b plots the variation of the peak of the beam size distribution under the influence of discharge power and argon flow rate in the absence of helium gas. Note that the size range variation is significantly narrower than in the presence of He. A comparison of Fig. 5a, b reaffirms that He plays the dominant role in shifting the nanocluster distribution toward smaller sizes.

Analogous conclusions are drawn from varying the aggregation length  $L$ . Figure 6a is a plot of the joint influence of  $L$  and  $Q_{\text{Ar}}$  at zero helium flow rate on the peak size of the nanocluster distribution. We see that the aggregation length plays the main role in changing the size, while there is little sensitivity to argon flow. In contrast, Fig. 6b, which follows the joint influence of  $L$  and  $Q_{\text{He}}$ , demonstrates a strong effect along both axes. The marked decrease in average particle size either with increasing He flow rate or with decreasing aggregation length confirms that the source residence time is the most sensitive parameter in determining the extent of particle condensation in the cold, strongly supersaturated, sputtered metal vapor environment, and that the dominant role of helium is in setting the transport time through the aggregation tube, as discussed above.

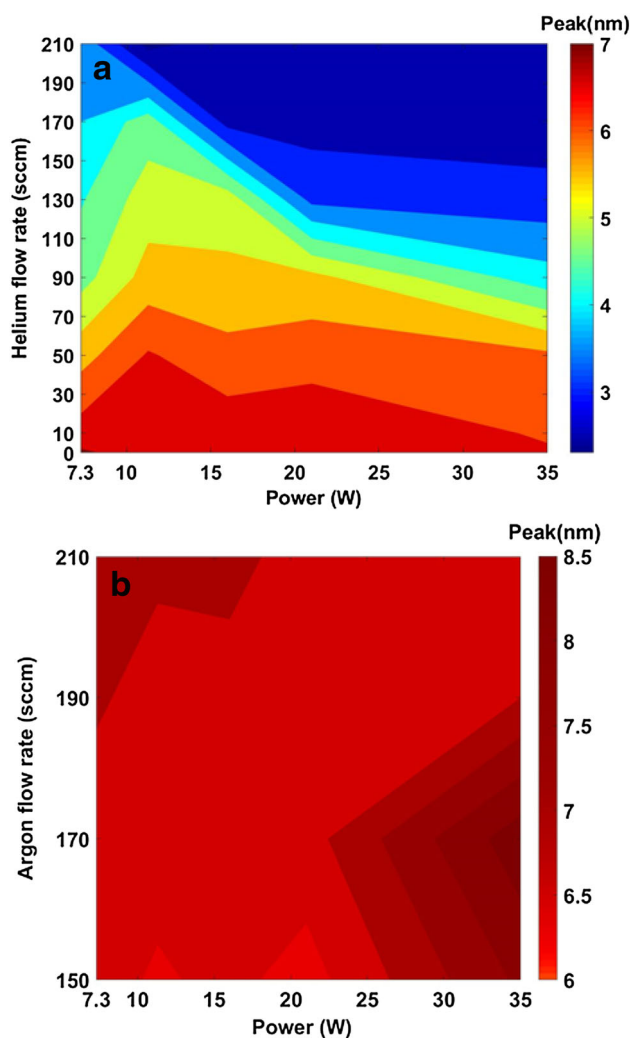


**Fig. 5** **a** Position of the peak of the Mn nanoparticle size distribution vs. magnetron discharge power and He flow rate. The flow rate was measured at intervals of 20 sccm, and the discharge powers and corresponding discharge currents were  $P = 7.3, 11.3, 15.8, 21.8, 35$  W and  $I = 35, 55, 75, 100, 150$  mA, respectively; the values in-between are interpolated. The argon flow rate was 190 sccm and the aggregation length was 9 cm. **b** The peak of the Mn nanocluster size distribution vs. magnetron discharge power and Ar flow rate. The flow rate intervals, and powers, discharge currents and the aggregation length were the same as in **a**. No helium flow was present for this plot

## Conclusions

We have presented a detailed study of the influence of the main operating parameters of a magnetron/condensation nanocluster source on the particle size. Specifically, we investigated how the peak size of the nanocluster ensemble responds to changes in the argon and helium gas supply flow rates, in the discharge power, and in the aggregation length. The benefit of such a cross-correlation study is that it allows one to classify the main physical role played by each of the variables.

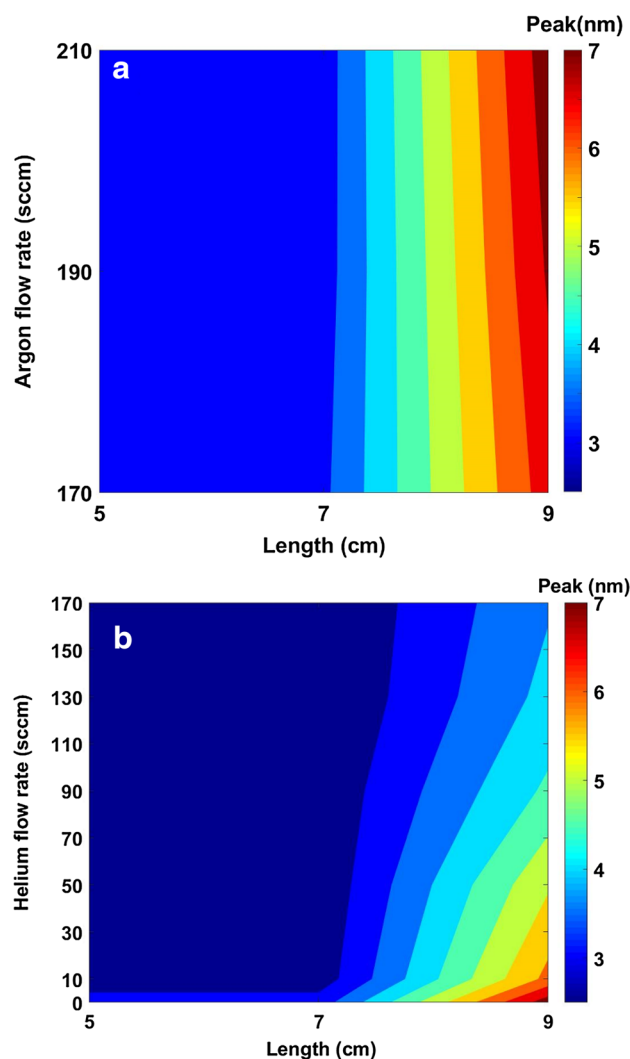


**Fig. 6** **a** The peak of the Mn nanocluster size distribution vs. the aggregation length and Ar flow rate. The flow rate was measured at intervals of 20 sccm, and the investigated lengths were 5, 7, and 9 cm. For this plot, no helium flow was present and the discharge power was 7.3 W. **b** The peak of the Mn nanocluster size distribution vs. the aggregation length and He flow rate. The flow rate intervals, the investigated aggregation lengths, and the power were the same as in **a**, and the Ar flow rate was 210 sccm

The sputtering power supplied to the discharge and the argon flow are the crucial parameters for nanocluster production. The discharge supplies the metal vapor for building the nanoparticles, while argon is not only responsible for the sputtering process but also is the dominant player in three-body collisions that provide the condensation nuclei triggering further growth.

Once the discharge and nucleation processes are stabilized, the next dominant factor is the source residence time, i.e., the length of time over which aggregation of the cryogenically cooled highly supersaturated metal vapor is allowed to proceed. If not terminated, it would result in the formation of large “smoke” particles both by addition of

individual atoms and by binary cluster–cluster collisions (Pfau et al. 1982; Zimmermann et al. 1994). Hence for obtaining a population of sufficiently small nanoclusters, it is essential to sweep the aggregating medium out of the source at an adequately fast rate. This is the main role of the helium supply. It is much less efficient than argon at promoting nucleation and aggregation, but an increase in the helium flow raises the pressure and density of the gas column inside the source, resulting in stronger entrapment of nanoparticles within the gas streamlines. This reduces their residence time and enhances the population of smaller particles in the beam.

A measurement of the kinetic energies of nanocluster ions exiting the source supports the preferential entrapment of smaller nanoclusters by the gas flow: 2 nm particles followed the terminal velocity of the gas expansion, while 9 nm ones displayed a significant velocity slip.

The two variables, the helium supply rate and the aggregation length (controlled by shifting the magnetron head with respect to the source exit aperture) have the dominant influence on the average nanocluster size in the outgoing beam.

The conclusions guided by systematic studies of source operation are useful for optimizing source performance, and are fruitful in untangling specific physical processes taking place within the dynamic sputtering/condensation source environment. It would be possible and interesting to gain further insight by exploring the above variables over a still wider range of values, as well as by adding new ones, for example other types of noble gases, variable sources of wall temperature, precise control of internal source pressure, etc., and by position- and time-resolved spectroscopy of the contents of the source interior.

**Acknowledgements** We would like to thank Dr. Avik Halder for extensive discussions, Akash P. Shah for valuable experimental assistance and for constructing the quadrupole ion deflector, the USC Machine Shop personnel for expert technical help, and the staff of Mantis Deposition Ltd. for their advice. This research was supported by the Army Research Office under Grant Number W911NF-17-1-0154.

**Open Access** This article is distributed under the terms of the Creative Commons Attribution 4.0 International License (<http://creativecommons.org/licenses/by/4.0/>), which permits unrestricted use, distribution, and reproduction in any medium, provided you give appropriate credit to the original author(s) and the source, provide a link to the Creative Commons license, and indicate if changes were made.

## Appendix: Cluster velocities

A measurement of cluster beam velocities was performed to examine the degree to which nanoparticles are susceptible to following the source gas streamlines.

During operation, the pressure of the argon and helium mixture inside the source is in the range of 10–100 Pa (Haberland et al. 1992; Hutte 2017). The source walls are cooled by liquid nitrogen, but the stagnation temperature at the exit aperture is expected to be higher. The corresponding mean free path  $l$  of the gas atoms lies in the range of  $\sim 0.05$ – $1.5$  mm (Haynes 2016). This corresponds to Knudsen numbers  $K_n = l/d \sim 0.01$ – $0.3$ , where  $d = 5$  mm is the diameter of the exit aperture, placing the expansion in the intermediate to mildly supersonic continuum regime (Hutzler et al. 2012). In this range, atoms and small molecules approach the regime of being fully accelerated by a buffer gas expansion (Hutzler et al. 2012); however, the “velocity slip” phenomenon (Milani and Iannotta 1999) also becomes more and more pronounced as the mass of the diluted species increases.

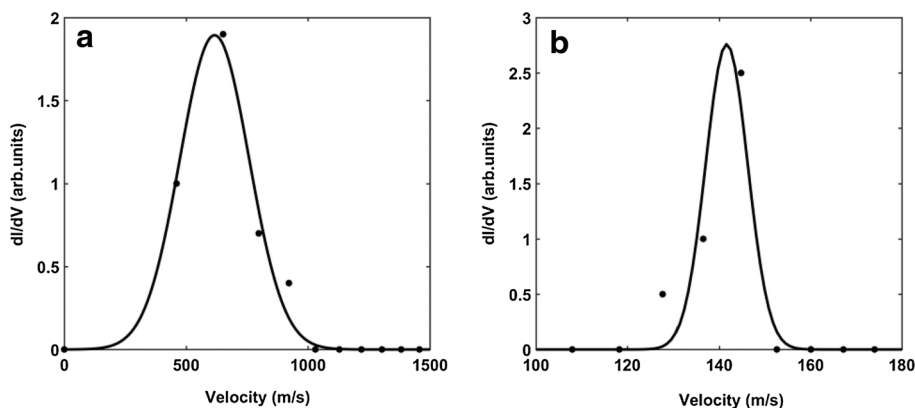
In the context of the present work, it is suggested that increased gas flow promotes the transport of nanoclusters through the interior of the aggregation volume. This decreases the time available for condensation and reduces the average cluster size in the outgoing beam. Therefore, one also would expect that for a given amount of gas flow and a given size distribution, the smaller clusters exit the nozzle with velocities closer to those of the helium and argon atoms, while the larger ones (which are prone to follow the streamlines less efficiently and therefore to spend longer within the condensation region) would exhibit a significantly larger velocity slip.

The velocities of negative cluster ions were measured by the retarding potential technique, using a Faraday cup with two grids, one to repel positively charged clusters and the other to apply a slowing voltage  $V$ . The current  $I$  of the ion beam was measured by the picoammeter and its kinetic energy distribution was determined by differentiating the  $I(V)$  curve and fitting the result with a Gaussian function. A complementary measurement of the ion energies utilizing a quadrupole beam deflector resulted in very close values. Details of these experimental arrangements will be described elsewhere.

The velocity distributions of Mn nanoparticles of 2 and 9 nm diameter are shown in Fig. 7. The gas flows for the two cases corresponded to molar fraction ratios within the source of  $X_{Ar}/X_{He} = 0.7$  and  $X_{Ar}/X_{He} = 3$ , respectively. The average velocity of the smaller nanoparticles is  $\sim 600$  m/s, while that of the larger ones is much lower,  $\sim 140$  m/s.

The terminal velocity for a gas mixture in the continuum expansion regime can be approximated (Cattolica et al. 1979; Miller 1988) by the use of an average mass  $\bar{M} = \sum X_i M_i$ , so that for monatomic gases, one has  $\bar{v}_t = (5k_B T_0 / \bar{M})^{1/2}$  [for a purely effusive expansion, the forward beam velocity is  $\approx 15\%$  lower (Pauly 2000;

**Fig. 7** Velocity distributions of Mn nanoparticles emitted by the source, as determined via retarding potential measurements. **a** Particle diameter 2 nm (aggregation length  $L = 9$  cm, Ar and He flow rates  $Q_{Ar} = 150$  sccm and  $Q_{He} = 210$  sccm, discharge power  $P = 15$  W). **b** Particle diameter 9 nm ( $L = 9$  cm,  $Q_{Ar} = 150$  sccm,  $Q_{He} = 50$  sccm,  $P = 15$  W)



Hutzler et al. 2012)]. The aforementioned velocity of 2 nm particles is in sensible agreement with the value  $v_i \approx 650$  m/s obtained for a stagnation temperature  $T_0 = 200$  K (as expected, this is somewhat higher than at the source jacket, see above), but the corresponding value for the 9 nm particle source parameters would be  $\approx 500$  m/s, which is significantly greater than the measured velocity. This implies that the larger nanoclusters display a significant velocity slip. Other groups (Ayesh et al. 2007; Polonskyi et al. 2012; Ganeva et al. 2013) have reported analogously low velocities and evidence of strong velocity slip for the heavier nanoclusters produced by magnetron aggregation sources. These observations support the picture of a more efficient transport of smaller nanoclusters by the gas flowing through the source.

## References

- Ayesh AI, Lassesson A, Brown SA, Dunbar ADF, Kaufmann M, Partridge JG, Reichel R, Lith JV (2007) Experimental and simulational study of the operation for a high transmission mass filter. *Rev Sci Instrum* 78:053906
- Ayesh AI, Qamhieh N, Ghamlouche H, Thaker S, El-Shaer M (2010) Fabrication of size-selected Pd nanoclusters using a magnetron plasma sputtering source. *J Appl Phys* 107:034317
- Ayesh AI, Ahmed HA, Awwad F, Abu-Eishah SI, Mahmood ST (2013) Mechanisms of Ti nanocluster formation by inert gas condensation. *Mater Res* 28:2622–2628
- Baker SH, Thornton SC, Keen AM, Preston TI, Norris C, Edmonds KW, Binns C (1997) The construction of a gas aggregation source for the preparation of mass-selected ultra-small metal particles. *Rev Sci Instrum* 68:1853–1857
- Binns C (2001) Nanoclusters deposited on surfaces. *Surf Sci Rep* 44:1–49
- Bray KR, Jiao CQ, DeCerbo JN (2014) Influence of carrier gas on the nucleation and growth of Nb nanoclusters formed through plasma gas condensation. *J Vac Sci Technol, B* 32:031805
- Cattolica RJ, Gallagher RJ, Anderson JB, Talbot L (1979) Aerodynamic separation of gases by velocity slip in free jet expansions. *AIAA J* 17:344–355
- Das SC, Majumdar A, Shripathi T, Hippler R (2009) Development of metal nanocluster ion source based on DC magnetron plasma sputtering at room temperature. *Rev Sci Instrum* 80:095103
- Dutka MV, Turkin AA, Vainchtein DI, De Hosson JThM (2015) On the formation of copper nanoparticles in nanocluster aggregation source. *J Vac Sci Technol, A* 33:031509
- Fischer A, Kruk R, Hahn H (2015) A versatile apparatus for the fine-tuned synthesis of cluster-based materials. *Rev Sci Instrum* 86:023304
- Ganeva M, Peter T, Bornholdt S, Kersten H, Strunskus T, Zaporotchenko V, Faupel F, Hippler R (2012) Mass spectrometric investigations of nano-size cluster ions produced by high pressure magnetron sputtering. *Contrib Plasma Phys* 52:881–889
- Ganeva M, Pipa AV, Smirnov BM, Kashtanov PV, Hippler R (2013) Velocity distribution of mass selected nano-size clusters. *Plasma Sources Sci Technol* 22:045011
- Gracia-Pinilla M, Vidaurri GS, Pérez-Tijerina E (2010) Deposition of size-selected Cu nanoparticles by inert gas condensation. *Nanoscale Res Lett* 5:180–188
- Haberland H (1994) Experimental methods. In: Haberland H (ed) *Clusters of atoms and molecules: theory, experiment, and clusters of atoms*. Springer, Berlin, pp 207–232
- Haberland H, Karrais M, Mall M, Thurner Y (1992) Thin films from energetic cluster impact: a feasibility study. *J Vac Sci Technol, A* 10:3266–3271
- Haberland H, Mall M, Moseler M, Qiang Y, Reiners T, Thurner Y (1994) Filling of micron-sized contact holes with copper by energetic cluster impact. *J Vac Sci Technol, A* 12:2925–2930
- Haynes W (ed) (2016) *CRC handbook of chemistry and physics*, 97th edn. CRC Press, Boca Raton
- Hihara T, Sumiyama K (1998) Formation and size control of a Ni cluster by plasma gas condensation. *J Appl Phys* 84:5270–5276
- Hutte Y (ed) (2017) *Gas-phase synthesis of nanoparticles*. Wiley-VCH, Weinheim
- Hutzler NR, Lu H-I, Doyle JM (2012) The buffer gas beam: an intense, cold, and slow source for atoms and molecules. *Chem Rev* 112:4803–4827
- Kappes M, Leutwyler S (1988) Molecular beams of clusters. In: Scoles G (ed) *Atomic and molecular beam methods*, vol 1. Oxford University Press, New York, pp 380–415
- Khojasteh M, Kresin VV (2016) Formation of manganese nanoclusters in a sputtering/aggregation source and the roles of individual operating parameters. *Proc SPIE* 10174:1017407
- Kusior A, Kollbek K, Kowalski K, Borysiewicz M, Wojcie T (2016) Sn and Cu oxide nanoparticles deposited on TiO<sub>2</sub> nanoflower 3D substrates by inert gas condensation technique. *Appl Surf Sci* 380:193–202



- Luo Z, Woodward WH, Smith JC, Castleman AW Jr (2012) Growth kinetics of Al clusters in the gas phase produced by a magnetron-sputtering source. *Int J Mass Spectrom* 309:176–181
- Mantis Deposition Ltd. Application Note App-001. [www.mantisdeposition.com/fileadmin/user\\_upload/images/appnotes/app\\_001.pdf](http://www.mantisdeposition.com/fileadmin/user_upload/images/appnotes/app_001.pdf). Accessed Jul 2017
- Meiwes-Broer K-H (ed) (2000) *Metal clusters at surfaces*. Springer, Berlin
- Milani P, Iannotta S (1999) *Cluster beam synthesis of nanostructured materials*. Springer, Berlin
- Miller DR (1988) Free jet sources. In: Scoles G (ed) *Atomic and molecular beam methods*, vol 1. Oxford University Press, New York, pp 14–53
- Morel R, Brenac A, Bayle-Guillemaud P (2003) Growth and properties of cobalt clusters made by sputtering gas-aggregation. *Eur Phys J D* 24:287–290
- Nielsen RM, Murphy S, Strebel C, Johansson M, Chorkendorff I, Nielsen JH (2010) The morphology of mass selected ruthenium nanoparticles from a magnetron-sputter gas-aggregation source. *J Nanopart Res* 12:1249–1262
- Pauly H (2000) *Atom, molecule, and cluster beams*. Springer, Berlin
- Pfau P, Sattler K, Muhlbach J, Pflaum R, Recknagel E (1982) Influence of condensation parameters on the size distribution of metal clusters. *J Phys F: Met Phys* 12:2131–2139
- Polonskyi O, Solar P, Kylian O, Drabik M, Artemenko A, Kousal J, Hanus J, Pesicka J, Matolinova I, Kolibalova E, Slavinska D, Biederman H (2012) Nanocomposite metal/plasma polymer films prepared by means of gas aggregation cluster source. *Thin Solid Films* 520:4155–4162
- Pratontep S, Carroll SJ, Xirouchaki C, Streun M, Palmer RE (2005) Size-selected cluster beam source based on radio frequency magnetron plasma sputtering and gas condensation. *Rev Sci Instrum* 76:045103
- Quesnel E, Pauliac-Vaujour E, Muffato V (2010) Modeling metallic nanoparticle synthesis in a magnetron-based nanocluster source by gas condensation of a sputtered vapor. *J Appl Phys* 107:054309
- Rudd R, Obrusnik A, Zikan P, Pratt R, Hall C, Murphy P, Evans D, Charrault E (2017) Manipulation of cluster formation through gas-wall boundary conditions in large area cluster sources. *Surf Coat Technol* 314:125–130
- Shyjumon I, Gopinadhan M, Helm CA, Smirnov BM, Hippler R (2006) Deposition of titanium/titanium oxide clusters produced by magnetron sputtering. *Thin Solid Films* 500:41–51
- Smirnov BM (2000) *Clusters and small particles*. Springer, New York
- Vajda S, White MG (2015) Catalysis applications of size-selected cluster deposition. *ACS Catal* 5:7152–7176
- Wegner K, Piseri P, Tafreshi HV, Milani P (2006) Cluster beam deposition: a tool for nanoscale science and technology. *J Phys D Appl Phys* 39:R439–R459
- Zhao J, Baibuz E, Vernieres J, Grammatikopoulos P, Jansson V, Negal M, Steinhauer S, Sowwan M, Kuronen A, Nordlund K, Djurabekova F (2016) Formation mechanism of Fe nanocubes by magnetron sputtering inert gas condensation. *ACS Nano* 10:4684–4694
- Zimmermann U, Malinowski N, Näher U, Frank S, Martin TP (1994) Producing and detecting very large clusters. *Z Phys D* 31:85–93

#### Publisher's Note

Springer Nature remains neutral with regard to jurisdictional claims in published maps and institutional affiliations.